HYDROLOGICAL PROCESSES
Hydrol. Process. **23**, 1221–1235 (2009)
Published online 4 February 2009 in Wiley InterScience
(www.interscience.wiley.com) DOI: 10.1002/hyp.7252

Simulating hydrologic and hydraulic processes throughout the Amazon River Basin

R. E. Beighley,[1]* K. G. Eggert,[2] T. Dunne,[3] Y. He,[1] V. Gummadi[1] and K. L. Verdin[4]

[1] *Civil, Construction and Environmental Engineering, San Diego State University, 5500 Campanile Drive, San Diego CA 92182-1324, USA*
[2] *Institute for Computation Earth System Sciences, University of California, Santa Barbara; formerly Theoretical Division, Los Alamos National Laboratory, Los Alamos, NM, USA*
[3] *Donald Bren School of Environmental Science and Management, University of CA, Santa Barbara, CA, USA*
[4] *US Geological Survey, Earth Resources Observation and Science Center, Sioux Falls, SD, USA*

Abstract:

Presented here is a model framework based on a land surface topography that can be represented with various degrees of resolution and capable of providing representative channel/floodplain hydraulic characteristics on a daily to hourly scale. The framework integrates two models: (1) a water balance model (WBM) for the vertical fluxes and stores of water in and through the canopy and soil layers based on the conservation of mass and energy, and (2) a routing model for the horizontal routing of surface and subsurface runoff and channel and floodplain waters based on kinematic and diffusion wave methodologies. The WBM is driven by satellite-derived precipitation (TRMM_3B42) and air temperature (MOD08_M3). The model's use of an irregular computational grid is intended to facilitate parallel processing for applications to continental and global scales. Results are presented for the Amazon Basin over the period Jan 2001 through Dec 2005. The model is shown to capture annual runoff totals, annual peaks, seasonal patterns, and daily fluctuations over a range of spatial scales ($>1,000$ to $<4{\cdot}7$M km^2). For the period of study, results suggest basin-wide total water storage changes in the Amazon vary by approximately $+/-5$ to 10 cm, and the fractional components accounting for these changes are: root zone soil moisture (20%), subsurface water being routed laterally to channels (40%) and channel/floodplain discharge (40%). Annual variability in monthly water storage changes by $+/-2{\cdot}5$ cm is likely due to 0·5 to 1 month variability in the arrival of significant rainfall periods throughout the basin. Copyright © 2009 John Wiley & Sons, Ltd.

KEY WORDS Amazon Basin; flood routing; hydrologic modelling

Received 9 July 2008; Accepted 3 December 2008

INTRODUCTION

Understanding the potential impacts of climate and land-use change at continental and global scales with a sufficient resolution for assessment and planning of water resources and related systems (such as ecological and biogeochemical cycles) requires accounting for spatial and temporal characteristics of hydrologic processes at a finer resolution than is possible in the current generation of Earth system models (Blöschl and Sivapalan, 1995; Beven, 2001). Significant advancement in understanding and predicting the magnitude, trend, timing and partitioning of terrestrial water stores and fluxes and hydrological hazards requires methods suitable for estimating inundation characteristics and water storage changes, which are unknown for much of the globe (Bates *et al*., 1997; Grayson *et al*., 2002). However, the origin of many land surface water cycle models is rooted in the need for a lower energy and mass flux boundary for the atmospheric component of global climate models (GCM). Consequently, land surface models incorporate only vertical column physics representations of the hydrologic cycle and energy balance processes, utilizing the same grid as the atmospheric circulation models. Most often, this grid is derived from latitude and longitude, so that the land surface representation is based on a rectangular discretization of the Earth's surface.

As GCMs have grown in sophistication, the land surface process representations have also become much more sophisticated to provide for differing vegetation, land use, and soil types, while still retaining the vertical, one-dimensional process structure. This approach has served well for modelling atmospheric circulation, and for the study of many associated hydrologic phenomena such as drought, the effects of plant cover on regional evaporation and precipitation, and other processes that can be reasonably characterized by vertical models. However, a growing interest in more complex research questions focused on understanding of the transfer and storage of water and energy in the Earth system; improving hydrologic model capability and performance through modern data assimilation techniques; and providing improved representations of ecosystem processes within global climate models, argues for the ability to realistically represent lateral transport of water and material on the land surface in a global model (Alsdorf *et al*., 2000; Alsdorf and Lettenmaier, 2003).

* Correspondence to: R. E. Beighley, Civil, Construction and Environmental Engineering, San Diego State University, 5500 Campanile Drive, San Diego CA 92182-1324, USA. E-mail: beighley@mail.sdsu.edu

Although numerous continental scale terrestrial water balance and/or transfer models exist (Catchment-LSM Koster *et al*., 2000; CLM Oleson *et al*., 2004; HYDRA Coe, 2000; LSX Costa and Foley, 1997; THMBv2 Coe *et al*., 2008; TRIP Oki and Sud, 1998; VIC-2L Liang *et al*., 1994; WBM/WTM Vorosmarty *et al*., 1996), these model frameworks are predominantly devoted to grid-based, vertical-column physics with limited hydraulic routing across land surfaces or through networks of channels and floodplain wetlands, with the exception of THMBv2 and TRIP, which provide representative channel cross-sections and Catchment-LSM which operates on an irregular grid. This paper presents a modelling framework based on a flexible method for systematically representing land surface topography with varying degrees of resolution and a fluvial transport system capable of providing representative channel and floodplain hydraulic characteristics (velocities, exchanges and storages) suitable for addressing research questions concerning inundation characteristics (extent, duration and frequency) and transmission characteristics (flow velocities and channel-floodplain exchange rates) for various components of a river basin. We demonstrate a framework by which the knowledge of land surface hydrology can be made available at a range of geographic scales and physical resolutions for linkages to be made between global climate models and the terrestrial resources that depend on the availability of water. We also present insights about the hydrological functioning of large river basins that can be further explored in a systematic manner as satellite-based data sources on such primary drivers as precipitation fields are improved.

STUDY SITE

This model was implemented on the Amazon Basin, the world's largest river basin (over 6 million km^2 or ~40% of South America). At peak flow, the discharge to the ocean is over 300 000 m^3 s^{-1}, and the annual flow of the Amazon accounts for approximately one fifth of the all river discharges to the oceans. Given the focus on modelling, and specifically on hydraulic routing, the Amazon Basin was selected due to its vast size, the limited number of hydraulic constraints along its reaches, and the critical role of its vast floodplain system in affecting storage and transmission of the flood wave (Richey *et al*., 1989) with important implications for biogeochemistry (Melack and Forsberg, 2001; Richey *et al*., 2002; Melack *et al*., 2004) and aquatic ecology (Goulding, 1981). The period of study, 1 January 2001 to December 31 2005, was selected to ensure continuous coverage of all the satellite-derived and remotely monitored datasets required to drive and assess the model. Central to this research are 34 streamflow gauges (Figure 1). The drainage areas for the selected gauges range from 1500 to 4·8 million km^2; mean annual peak discharges for the period of study range from 170 to 250 000 m^3 s^{-1}; and mean annual runoff ranges from 520 to 3300 mm. The daily gauge data are used to assess the model results.

METHODOLOGIES

Landscape representation

A key feature of our approach is the topographic method used to subdivide the landscape and define the

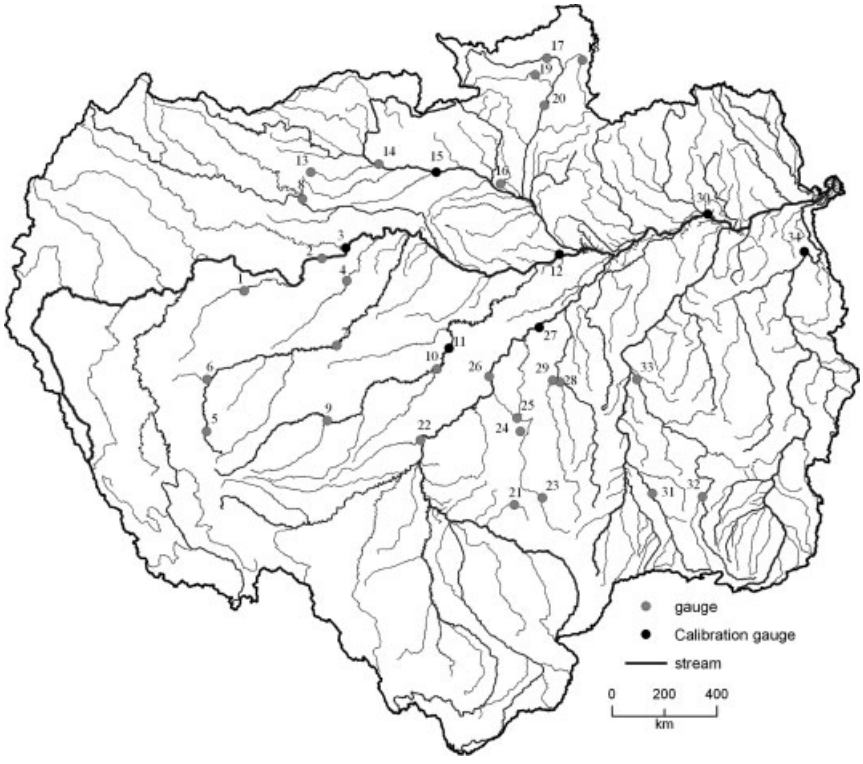

Figure 1. Amazon Basin derived from SRTM 3 arcsec DEM, with the locations of the 34 flow gauging sites (listed in Table I), including the seven calibration sites, used in this study

DOI: 10.1002/hyp

model unit boundaries (i.e. irregular computational grid). The discretization framework used for this study is based on concepts first articulated by Pfafstetter (1989) and implemented for the globe by Verdin and Verdin (1999). This framework is a natural system, based on topographic subdivision of the land surface and the resulting topology of the hydrographic network. Some of the appeal of the Pfafstetter approach stems from its economy of digits used to number the topographic units, the topological information that the digits carry, and the facility with which it lends itself to computational parallelization.

Central to the Pfafstetter decomposition method are basins and interbasins. Basins are defined as the four largest tributaries discharging to the main stem of a given drainage system, where the main stem is defined as the drainage path that follows the maximum drainage area from the network outlet to the drainage divide. Interbasins are defined as the five areas drained by the main stem between tributary confluences. Thus, for a level-1 delineation, a watershed is divided into nine units (Figure 2). For each successive level, each unit is further subdivided into an additional nine units (i.e., maximum number of model units $= 9^{\text{Level.}}$). The subdivision process is limited only by the detail and accuracy of the underlying drainage network. The product of this recursive subdivision is a set of independent hydrologic drainages that do not exchange water except through the stream network (i.e. nodes). The number assigned to each of the independent stream and drainage units provides not only an identifying number for the unit, but also contains all of the information needed to determine where the unit resides topologically in the global stream network. Thus, the lack of exchange of surface water except at pour points combined with the topology built into the Pfafstetter number system provides a natural parallelism that can be exploited using parallel computing.

In this study, surface topography is approximately by the second version of the 3-arcsec (~90 m) digital elevation model (DEM) developed from NASA's Shuttle Radar Topography Mission (SRTM) (Farr *et al.*, 2007). The DEM was used to define flow directions, ground slopes and the resulting drainage network (Moglen and Beighley, 2000). Note, STRM vertical accuracy is on the order of 1 to 10 m and is impacted by vegetation and other artefacts. For the purpose of identifying channel locations and sub-basin boundaries, these limitations are not significant. However, SRTM derived channel slopes are problematic and need to be filtered (see Model parameterization). Figure 2 shows the Amazon Basin delineated to Pfafstetter level 4 (i.e. maximum of 9^4 or 6561 model units) using a threshold area of 8·1 km^2. The resulting number of basins and interbasins is 5189, which is less than the upper limit of 6561 due to limitations in the derived drainage network. At level 4, the median model unit drainage area is 240 km^2 ranging from <1 to 43 300 km^2.

Model framework

The model is built on an irregular computational grid as defined by the Pfafstetter decomposition method and

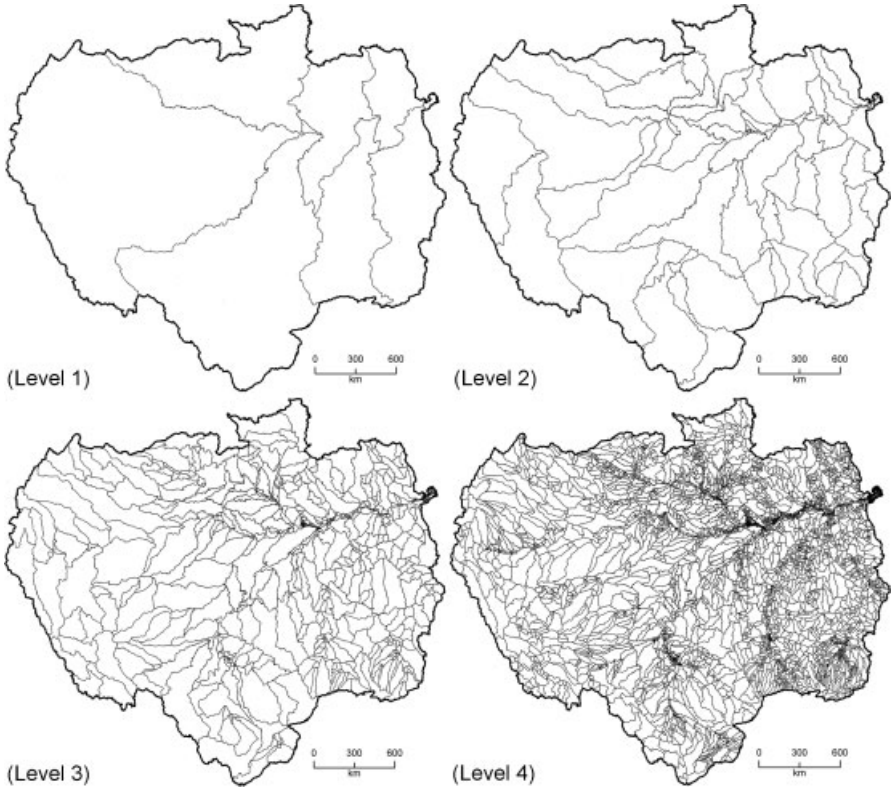

Figure 2. Delineation of the Amazon Basin at: Level 1 [9 units; median area = 498 500 km^2]; Level 2 [81 units; 37 100 km^2]; Level 3 [707 units; 1990 km^2]; and Level 4 [5189 units; 240 km^2]

DOI: 10.1002/hyp

consists of three main components: data remapping, vertical water balance, and horizontal routing of surface, subsurface, channel and floodplain waters. Once the overall watershed is subdivided to the desired level, each of the Pfafstetter basins and interbasins are transformed into a system of open-book watershed approximations connected at upstream and downstream junction points (Wooding, 1965). Each open-book system consists of an included channel reach bordered by a plane on each side. Figure 3 illustrates the transformation of the SRTM derived basin and channel boundaries to the planes (i.e. surfaces that discharge laterally to the channel/floodplain) and channel/floodplain segments. The draining surfaces represented in this way are not necessarily individual hillslopes (except at high levels of landscape representation) but more commonly are ridges or even groups of similar tributary catchments fretted into a regional topographic trend. The flexibility to represent topography by this open-book approximation with varying degrees of resolution allows the method to be used to systematically investigate the influence of topography, drainage density, and flow path lengths on runoff response. In the water balance model, the irregular boundaries derived from SRTM are maintained. For the routing model, the irregular boundaries are approximated as rectangular elements. The down gradient plane length, L_p, is approximated as $L_p = A_p/L_c$, where A_p is the area of the plane obtained from the DEM delineation and L_c is the length of the channel, which is also the width of each plane, as measured from the DEM in the Pfafstetter unit.

Data remapping. Data remapping is required to transform the available datasets, which are obtained in the form of rectangular grids, to the irregular computational grid. For any given dataset, model parameters are spatially averaged, $\overline{X}$, to the scale of the basin and interbasin plane elements (Figure 3):

$$\overline{X} = \sum_{i=1}^{m} (X_i A_i) \div A_p \tag{1}$$

where X_i is the data value in region i of a plane element within a model unit, A_i is the area of region i, m is the number of unique data regions in boundary of a plane element, and A_p is the area of a plane element within a model unit. To facilitate data transformation, specifically for time series data, an index system is created for each model unit plane that contains the number of grid cells required to completely cover the plane (m), their locations within the grid (x, y), and their corresponding overlapping areas (A_i). Thus, it is possible to drive the model with the original rectangular data and the index file, which can be efficiently accomplished within a GIS.

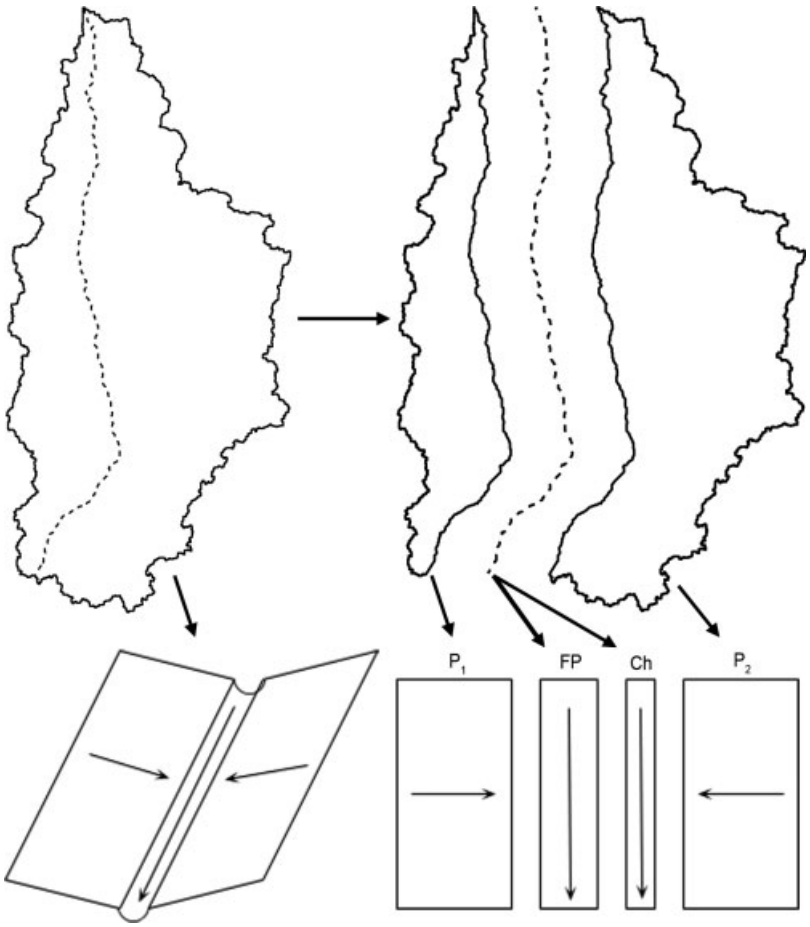

Figure 3. Transformation of the irregular computation grid to rectangular units

DOI: 10.1002/hyp

Water balance model. The focus of this paper is on the combined use of the irregular computation grid and the horizontal routing models. Therefore, the simple water balance model, WBM, used in this research is presented only for completeness, with the notion that the routing model can be adapted to another vertical WBM of any desired complexity. The conceptual framework for the WBM used here is shown in Figure 4 and described in Appendix A. The WBM represents the vertical fluxes and stores of water in and through the canopy and soil layers based on the conservation of mass and energy. The subsurface zone is separated into two layers: the upper layer or root zone supporting evapotranspiration, and the lower layer, which may consist of saprolite and permeable bedrock, supporting horizontal routing. The upper layer is characterized by a rooting depth and a plant-available water capacity; the lower layer by a hydraulic conductivity and drainable porosity. The canopy is characterized by leaf area index (LAI), resistance factors for the impedance of vapour transport, and a precipitation interception factor. Evapotranspiration (ET) is the sum of wet canopy evaporation, dry canopy transpiration and evaporation from saturated soil surfaces based on the potential ET using Penman–Monteith indirectly through the temperature-based method of estimating its data sources developed by Allen *et al.* (1998). Infiltration is total precipitation minus canopy interception and the fraction of precipitation falling on saturated surfaces. In landscapes where infiltration-limited overland flow is expected, the precipitation must be concentrated into realistic storm durations and an infiltration capacity estimated. However, in the Amazon Basin, infiltration-limited overland flow is confined to deforested hillslopes (de Moraes *et al.*, 2006), which we do not treat in this implementation. Accretions to the lower soil layer occur when infiltration exceeds the sum of ET and the root zone moisture deficit. In each time step, the WBM passes two sources of water to the routing model: water available for surface runoff (T_s) and water transferred to the lower soil layer (D); both quantities have units of depth per time and are integrated over plane area in the routing model. The water balance of the lower soil layer is performed by the routing model.

River and hillslope routing models. Routing is performed using one-dimensional equations for flow. In particular, the methods used are: (a) the kinematic wave method for surface and subsurface runoff from plane elements; (b) the kinematic wave method for first-order tributary channels; and (c) Muskingum–Cunge (MC) routing for interbasin channels and floodplains. These methods are well proven and described by numerous authors (Chow, 1959; Mahmood and Yevjevich, 1975; Maidment, 1992).

The subsurface flow (q_{ss}) model uses the simple Dupuit approximation that equates the slope of the phreatic surface with the head gradient. Further, a kinematic assumption is made that equates the head gradient to the slope of the plane surface (Eagleson, 1970). The

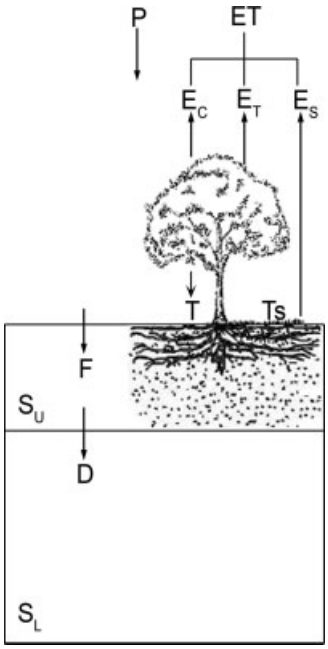

Figure 4. Conceptual framework (defined in Equation (A-1)) for the water balance model

continuity equation for the subsurface flow is derived to develop the subsurface routing scheme. Beginning with Darcy's Law, $u = -K\frac{\partial h}{\partial x_p}$, where u is the mean horizontal velocity of subsurface flow, K is hydraulic conductivity, h is the depth of saturated flow in the aquifer, and x_p is the distance down a plane element. By making the kinematic assumption, $\frac{\partial h}{\partial x_p} = -S_p$, where S_p is the surface slope of plane element and noting that $q_{ss} = uh$, $q_{ss} = KS_p h$ and has units of discharge per unit width of the plane. However, the effective depth of flow is $h^* = \phi h$, where ϕ is the porosity. Therefore, $q_{ss} = KS_p h^*/\phi$, and the continuity equation is:

$$\frac{\partial q_{ss}}{\partial x_P} + \frac{\partial h^*}{\partial t} = D(t) \tag{2}$$

where x_P is the distance down a plane and $D(t)$ is the rate with which water percolates vertically into the lower soil layer delivered from the WBM. In subsequent development we use the common expression for discharge per unit width of plane as a function of flow depth, $q_{ss} = \alpha(h^*)^\beta$. In the case of subsurface flow, $\alpha = KS_p/\phi$ and $\beta = 1$.

In many watersheds, shallow subsurface water can saturate the entire soil column and a portion of it reemerges onto the land surface. The water then flows to the stream network as saturation overland flow (Dunne and Black, 1970; Dunne, 1978). This phenomenon is observed in the Amazon basin (de Moraes *et al.*, 2006). Therefore, after the subsurface calculation is complete for the current plane, a check is made to determine if the subsurface depth of flow is greater than the total soil layer thickness, H, for each Δx_P down the plane slope. If so, the excess water is added to any surface water excess for this time step (Figure 5).

DOI: 10.1002/hyp

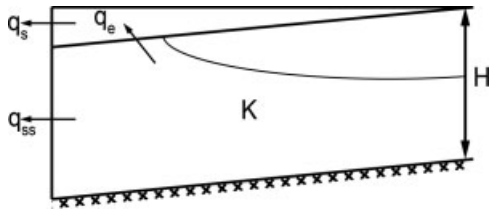

Figure 5. Conceptual framework for the surface and subsurface routing model showing surface (q_s), subsurface (q_{ss}) runoff, soil thickness (H), re-emergence of subsurface flow as (q_e), and horizontal hydraulic conductivity (K)

The surface runoff (q_s) model is based on the continuity equation for overland flow:

$$\frac{\partial q_s}{\partial x_P} + \frac{\partial y}{\partial t} = T_s(t) \tag{3}$$

where q_s is the surface runoff per unit width of the plane element, x_P is the distance down a plane, y is the notional mean depth of surface flow and $T_s(t)$ is the rate of water available for surface runoff delivered from the WBM. Using the Darcy–Weisbach resistance equation for overland flow, $S_f = f\frac{q_s^2}{8gy^3}$, where f is the Darcy–Weisbach friction factor that varies with vegetation density and microtopography (Dunne and Dietrich, 1980), and the kinematic assumption, $S_f = S_p$, where S_p is the slope of plane element, provides an expression for the surface discharge per unit width of the form $q_s^2 = \alpha y^\beta$; that is:

$$q_s^2 = \frac{8gS_p}{f} y^3 \tag{4}$$

With expressions for both q_s and q_{ss} known, it is possible to calculate channel discharge (Q_c) for the current time step. The continuity equation for channel flow is:

$$\frac{\partial Q_c}{\partial x_c} + \frac{\partial A_c}{\partial t} = q_s + q_{ss} = q_l \tag{5}$$

where A_c is the cross-sectional area of flow in the channel and q_l is the lateral inflow to the channel, and x_c is distance down a channel. In Equations (2) and (3), q_s and q_{ss} are in terms of discharge per unit width of plane element, which is the same as per length of channel as used in Equation (5) (Figure 3).

For the first-order tributary basin channels, the kinematic wave assumption and Manning's equation (Chow, 1959) relate Q_c and A_c:

$$Q_c = \frac{1}{n} R_c^{2/3} S_o^{1/2} A_c \tag{6}$$

where n is the Manning resistance parameter, R_c is the hydraulic radius, defined as $R_c = \frac{A_c}{P_c}$, where P_c is the wetted perimeter of the channel, and S_o is the channel bed slope.

In many approaches for hydrologic modelling of basins, P_c is expressed as a function of A_c through a regression of cross-sectional survey data. Such expressions take the form $P_c = a_1 A_c^{b1}$. However, in the case of the example used herein, such relationships are not known. For this situation, first-order tributary channels are assumed triangular based on the surface slopes of the two contributing plane elements and P–A relationships are derived for each channel. With the relationship between P_c and A_c defined, Equation (6) can be expressed in the form:

$$Q_c = \alpha_c A_c^{\beta_c} \tag{7}$$

where

$$\alpha_c = \frac{S_o^{1/2}}{a_1^{2/3} n} \text{ and } \beta_c = \left(\frac{(5 - 2b_1)}{3}\right).$$

Analytical solutions for Equations (2), (3) and (5), were first discussed by Harley *et al.* (1970), and numerical solutions to the problem were presented by Eggert (1980, 1987), and many others. In this formulation, Equations (2), (3) and (5) are solved using the finite-difference scheme presented by Li *et al.* (1975).

For interbasin channel/floodplain reaches, the Muskingham–Cunge (MC) routing method is used. These channels have bed slopes much less than 0·001, smaller than are appropriate for kinematic wave approximations. Flatter bed slopes increase the importance of the diffusive processes in wave propagation. The MC approach provides a solution that allows one to use its inherent numerical diffusion to approximate the diffusion term of the Saint Venant Equation; $S_f = S_o - \frac{\partial y}{\partial x}$. The iterative MC method with constant parameters as presented by Ponce and Yevjevich (1978) is used here to calculate discharge in both floodplain and main channel representations for each reach. The equations for both are similar to Equations (5), (6) and (7). A method, based on that developed by Garbrecht and Brunner (1991), divides the inflow from an upstream channel reach into a channel discharge and floodplain discharge, and routes these flows separately. Given the scale of simulation, their method was modified to use a wide-channel approximation. If upstream inflows can be conveyed by the main channel at less than bankfull depth, then all flow is routed through the main channel. When discharge exceeds the bankfull capacity of the channel, a portion of it is routed along the floodplain using the MC method. Once there is floodplain flow, it is further assumed that if the upstream discharge falls below the capacity of the channel at bankfull depth, water already in that floodplain reach will continue to flow in the floodplain until it has been completely routed to the next downstream reach where it can re-enter the channel (i.e. it does not drain back to the channel within its reach length).

In this framework, representative, reach-averaged cross-sections are required for all interbasin channel/floodplain reaches. The purpose here is not to specify every local variation of cross-section shape but to capture the influence of broad, physiographic trends. A wide rectangular cross-section is assumed, which is supported by measured cross-sections discussed in Coe *et al.* (2008)

DOI: 10.1002/hyp

for the Amazon Basin. The representative location along the reach is assumed to be the point that approximates the geometric mean of the drainage areas at the upstream and downstream ends of the reach (Beighley and Moglen, 2003):

$$A_r = 10^{[Log(A_u)+Log(A_d)]/2} \quad (8)$$

where A_r is the representative drainage area (km^2), A_u is the drainage area at the most upstream point along the reach, and A_d is the drainage area at the most downstream point along the reach. Next, bankfull depth, d_b, and width, w_b, and floodplain width, w_f, are approximately based on the relationships presented in Gummadi (2008), which were developed using data from 82 stream gauges distributed throughout the Amazon basin and the floodplain inundation maps presented in Hess *et al.* (2003):

$$d_b = 0{\cdot}25\ A_r^{0.34} \quad (R^2 = 0{\cdot}71) \quad (9)$$

$$w_b = 2{\cdot}36\ A_r^{0.47} \quad (R^2 = 0{\cdot}80) \quad (10)$$

$$w_f = 0{\cdot}017\ A_r^{0.96} \quad (R^2 = 0{\cdot}88) \quad (11)$$

where width and depth are in metres. Note, Equations (9) and (10) are similar to those presented by Coe *et al.* (2008): $d_b = 0{\cdot}15A^{0.40}$ and $w_b = 0{\cdot}42A^{0.59}$, for the Amazon Basin, with the above producing slightly smaller channel dimensions for large drainages.

Hydraulic routing is performed for the entire basin in each time step (e.g. 15 min). The WBM, in its current form, calculates the daily availability of water for routing on the surface and subsurface from each plane. Given that routing is performed on a finer time step, the daily surface and subsurface values are divided by the number of time steps needed for routing (e.g. the routing model time step is 15 min, requiring 96 routing model time steps per daily WBM time step). For each routing time step, the sequence of calculations within a given model unit are subsurface, surface, channel/floodplain routing, starting at the top of the watershed and working downstream using the Pfafstetter numbering system.

Model parameterization. In the current form, the WBM requires four spatially distributed datasets: LAI, root zone soil thickness, rainfall and temperature. Several uniformly distributed model parameters used for calibration are also described in Appendix A. LAI data (MOD15_BU) were obtained from the Moderate Resolution Imaging Spectroradiometer (MODIS) aboard the Terra satellite as monthly grids with at 1 km horizontal resolution (Yang *et al.*, 2006). Gridded soil thickness data were estimated at a 1° horizontal resolution (Webb *et al.*, 2000). The precipitation data were obtained from NASA's Tropical Rainfall Measuring Mission (TRMM). The TRMM data (3B42) were obtained as grids with a horizontal resolution of 0·25° (27 km) every 3 h (Huffman *et al.*, 2007), aggregated to daily totals and spatially averaged to the boundary of each model plane. Air temperature data (MOD08_M3) were obtained from the MODIS aboard the Terra satellite. The temperature data were obtained as monthly grids with a horizontal resolution of 1° (Seemann *et al.*, 2003). The monthly data provide mean, minimum and maximum values based on daily air temperatures at a vertical pressure level of 1000 hPa and were assumed sufficient to capture the seasonal variability for the *ET* model.

The routing model requires ten input variables: hillslope, channel and floodplain length and gradient; bankfull channel width and depth; floodplain width; subsurface soil thickness, and four parameters: hillslope, channel and floodplain roughness and horizontal conductivity. All length terms were determined using the 90 m SRTM DEM, and channel and floodplain lengths were assumed to be identical (that is, the effects of channel sinuosity are contained within the hydraulic roughness for each reach). Hillslope gradients were approximated as the mean of the individual pixel slopes for all pixels within the hillslope region, where pixel slopes were determined using the DEM. Channel and floodplain gradients were assumed to be identical and approximated as the mean of the individual pixel slopes along the channel reach. Due to the vertical accuracy (±7 m) and limitations of the SRTM, especially over open water, slopes resulting in bankfull channel velocities less than 0·3 m s^{-1} or greater than 2 m s^{-1} (based on Manning's equation) were either increased or decreased to ensure bankfull velocities were within that range. For example, slopes along the mainstem of the Amazon River are on the order of 1 to 10 cm km^{-1}. Due to vertical accuracy, SRTM elevation can vary by several metres over a relatively short reach lengths resulting in potentially negative or very steep slopes. These slopes were adjusted to ensure reasonable flow velocities (Gummadi, 2008). Future NASA mission such as the Surface Water and Ocean Topography (SWOT) mission will enable channel surface slopes to be obtained remotely and at much greater accuracy reducing model uncertainty and calibration demands (see http://bprc.osu.edu/water/and Alsdorf *et al.*, 2007). Hillslope, channel and floodplain roughness terms were initially approximated based on literature values and adjusted by calibration. Effective subsurface thickness (H in Figure 5) was initially estimated based on limited field data, but both soil thickness and horizontal conductivity were calibrated.

RESULTS AND DISCUSSION

The focus of this paper is on the routing model. The discussion of the WBM results is intended to support the appropriateness of the inputs to the routing model. A rigorous assessment is presented for the routing model, where results are evaluated at 34 gauge locations with drainage areas ranging from 1500 to 4·8 million km^2. Discharge data were obtained from the Brazilian Water Agency: Agéncia Nacional de Águas (ANA, www.ana.gov.br). The calibration process (datasets and objective functions) is discussed in detail for the routing

DOI: 10.1002/hyp

model. The uniqueness of the model, tracking of all water storages at a fine spatial and temporal resolution, is also illustrated.

Water balance model

The WBM was calibrated using two parameters: maximum soil moisture deficit (i.e. usable soil moisture, calibrated to 10%) and the fraction of rainfall intercepted by the canopy (calibrated to 15%). In general, as these terms increase, *ET* also increases. The WBM and routing model can be run separately or coupled, so the preliminary calibration of the WBM was performed separately from the routing model and relied on the assessment of simulated *ET* values and runoff : rainfall, $Q:P$, ratios relative to reported values. Note, for this analysis the value of Q is defined as the sum of the two sources of water passed to the routing model (T_s and D in Figure 4). Following the preliminary calibration, the models were coupled and the calibration focused on the comparison of streamflow statistics at select gauge locations.

From the calibrated WBM averaged over entire Amazon Basin for the period of analysis, basin-wide mean annual rainfall ranged from 1990 to 2040 mm: similar to the 2130 mm year^{-1} presented by Costa and Foley (1998) from a multi-dataset (gauges, remote sensing and reanalysis), multi-year analysis. The lower annual rainfall may be attributed to differences in study periods and/or the potential for TRMM 3B42 to underestimate precipitation in the Amazon Basin (de Goncalves *et al*., 2006). For individual model units, annual rainfall ranged from 270 to 4180 mm. Basin-wide *ET* averaged over a year ranged from 2·6 to 3·0 mm day^{-1}; 0·4 to 4·6 mm day^{-1} for individual model units. These *ET* values are comparable to observed estimates of actual values: 2·9 to 3·8 mm day^{-1} (Costa and Foley, 1997). Basin-wide $Q:P$ ratios averaged over a year ranged from 45 to 52%, which are also comparable to reported values: 45–47% (Vorosmarty *et al*., 1996; Costa and Foley, 1997). As shown above, the WBM is driven by reasonable precipitation as obtained from TRMM (3B42) and provides typical values of runoff and *ET*.

Hydraulic routing model

The routing model was calibrated by adjusting five parameters in order to minimize mean model error based on daily data from seven streamflow gauges (Figure 1) and four measures of error: normalized relative error (NRE), normalized root-mean-squared error (NRMSE), mean annual daily peak discharge error (E_{Qp}), and mean annual runoff error (E_Q). The objective function for the calibration process was the mean of the four error measures. The seven calibration gauges were selected to assess streamflow from major tributaries throughout the basin. The calibrated parameter set consists of the Darcy–Weisbach friction factor for overland flow ($f = 10\,000$); Manning's channel ($n = 0{\cdot}04$) and floodplain ($n = 0{\cdot}07$) roughness; horizontal conductivity ($K = 0{\cdot}05$ m s^{-1}) and subsurface soil depth ($H = 5$ m). The mean model error for the seven calibration sites is 3·5% (NRE $= -4{\cdot}2$, NRMSE $= 15{\cdot}6$, $E_{Qp} = 4{\cdot}9$ and $E_Q = -2{\cdot}2\%$), with a Pearson correlation coefficient, R, of 0·87. The error measures are similar for the calibration gauges with mean errors ranging from −2 to 5%, except for the Purus gauge (13 880 000) with a mean error of 13%. Considering all the gauges, there is no scale dependence or spatial pattern to the model errors. Table I lists the error measures for all 34 sites.

The thickness of the soil-saprolite aquifer that conveys most subsurface flow in the Amazon basin mainly influenced peak discharges at the onset of the rainy season and the timing of initial hydrograph rise in small (<10 000 km^2) basins. Hydrograph predictions are not sensitive to the Darcy–Weisbach friction estimates because of the small amount of overland flow. In contrast, channel and floodplain roughness and horizontal conductivity have a strong influence on simulated hydrographs. It is therefore especially important that calibrated channel roughness (0·04) is similar to values reported in the literature for channels (Chow, 1959), and calibrated floodplain roughness (0·07) is only slightly smaller than published values for wooded floodplains (Arcement and Schneider, 1989) perhaps because of the relatively low density of understory vegetation beneath Amazon forest canopies and the large areas of open water in lakes and floodplain channels (Sippel *et al*., 1991; Mertes and Dunne, 2008, Figures 8·7–8·11). The comparison between the calibrated and reported roughness values suggests that the slope and geometry of the second- and higher-order channels used in the kinematic and MC routing equations are approximately correct. However, the calibrated value for horizontal conductivity is 3–4 orders of magnitude larger than typical values (Rawls *et al*., 1983). The primary reason for the elevated value is related to the resolution of the current model. The current hillslope length scale (∼10 km) that is determined by the chosen Pfafstetter resolution is more than 10 times larger than most Amazon basin hillslopes. In reality, subsurface water reaches a channel after travelling a shorter distance than is represented in the current model. Thus, in the current implementation of the model at Pfafstetter level 4 (Figure 2), K must be increased to account for the longer subsurface flow paths. Future efforts will specifically investigate this scaling issue using a finer scale model.

Based on data from 27 stream gauges not used in the calibration process, mean model error is 9·1% (NRE $= -0{\cdot}5$, NRMSE $= 22{\cdot}5$, $E_{Qp} = 5{\cdot}9$ and $E_Q = 8{\cdot}3\%$), with $R = 0{\cdot}77$ (Table I). These errors relate to daily values, suggesting that the simulated response timing is good, especially for the smaller basins. Figure 6 shows the comparison between the modelled and gauged discharge at six locations selected to represent the spatial scales captured by the model: ∼1000 s to 4·7 million km^2. The figure shows that the timing of the simulated hydrographs generally matches the gauge data.

To illustrate the importance of routing at a daily resolution for even large drainages, Figure 7 shows 30-day blocks of daily data for selected periods from

DOI: 10.1002/hyp

Table I. Summary statistics for simulated streamflow at the 34 study gauge locations shown in Figure 1; normalized relative error (*NRE*), normalized root mean squared error (*NRMSE*), mean error in annual peak discharge (EQ_p), mean error in annual runoff (*EQ*), and correlation between simulated and measures daily streamflow (*R*)

ID	Gauge No.	Area (km^2)	*NRE* (%)	*NRMSE* (%)	*EQp* (%)	*EQ* (%)	*R*
1	10 300 000	25,900	47	51	83	90	0·78
2	11 400 000	1,033,500	−8	16	−6	−5	0·83
3	11 500 000*	1,159,900	−5	16	−2	−3	0·83
4	12 200 000	37,100	−13	35	−10	−19	0·35
5	12 360 000	10,200	10	17	−47	95	0·42
6	12 500 000	41,300	25	31	16	96	0·62
7	12 700 000	149,100	32	37	53	67	0·85
8	12 845 000	209,300	−19	22	−20	−28	0·89
9	13 410 000	65,000	3	17	−14	15	0·66
10	13 870 000	233,000	10	22	35	25	0·88
11	13 880 000*	242,100	4	18	20	11	0·89
12	14 100 000*	2,230,400	−10	18	−3	−6	0·84
13	14 260 000	41,800	−1	11	−7	1	0·87
14	14 330 000	196,000	−8	17	−6	−17	0·86
15	14 420 000*	296,200	−12	21	0	−15	0·86
16	14 440 000	16,300	−1	13	17	8	0·87
17	14 495 000	37,200	−3	19	31	−11	0·89
18	14 526 000	10,200	7	15	−19	64	0·79
19	14 680 001	13,500	9	31	61	31	0·82
20	14 710 000	127,500	6	19	39	30	0·92
21	15 170 000	1,500	4	12	−4	35	0·71
22	15 320 002	962,500	11	20	38	29	0·89
23	15 558 000	10,400	−11	20	−39	−41	0·53
24	15 575 000	5,700	−9	22	23	−10	0·64
25	15 580 000	66,200	−13	24	−40	−33	0·60
26	15 630 000	1,138,600	4	12	13	16	0·93
27	15 700 000*	1,195,000	−0·2	12	8	2	0·92
28	15 800 000	71,700	−11	19	−11	−28	0·84
29	15 828 000	61,000	−15	23	−30	−46	0·82
30	17 050 001*	4,779,200	−3	13	4	−1	0·92
31	17 120 000	38,500	−21	29	29	−46	0·77
32	17 280 000	38,000	−29	35	−1	−48	0·75
33	17 420 000	142,900	−17	20	−23	−44	0·92
34	18 850 000*	460,200	−2	12	8	−3	0·87

* Included in calibration set

the hydrographs in Figure 6. Four important features are illustrated in Figure 7: (1) the model captures peak discharges (Figure 7a, b, c) and the transition from falling to rising discharge (Figure 7b, e, f) with timing errors ranging from 0–10 days; (2) for areas up to 100 000s of km^2, hydrographs can rise, peak and fall in 1–5 days; and (3) for watersheds draining more than a million km^2, changes in discharge occur more near the weekly scale. Figure 7 also shows the comparison between monthly averaged and daily discharges. At the monthly scale, the actual variability in streamflow hydraulic characteristics (e.g. discharge and corresponding velocity and depth) is muted, even at Obidos. For the selected gauges and periods shown in Figure 7, observed and simulated changes in discharge lie in the range 0·001–0·0001 m^3 s^{-1} km^{-2} day^{-1}.

Combined model results

Combining the results from the two models, Figure 8 shows the spatial distribution of monthly water storages changes for the period January 2005 to December 2005 relative to mean monthly storage for the period April 2002 to December 2003. The reference period was selected, not for its hydrological value, but as a link to NASA's Gravity Recovery and Climate Experiment (GRACE) mission (Tapley *et al.*, 2004). For 2005, the basin-wide maximum positive and negative changes in water storage occurred in May 2005 (+4·1 cm) and November (−9·3 cm), respectively. These changes are similar to those presented by Rodell and Famiglietti (1999) for the Amazon based on results from 10 different water balance models: +4 to +10 cm in April/May and −5 to −10 cm in October/November. This timing is also captured by GRACE, which shows a maximum positive and negative change in geiod height occurring in April 2003 and October 2003, respectively (Tapley *et al.*, 2004). In Figure 8, the combined storage changes include variations in root-zone soil moisture, surface and subsurface flow, and channel and floodplain flow within each model unit. The monthly variation of these totals averaged over the basin is shown in Figure 9. On average, the annual variability in water storage changes is +/−5 to 10 cm. The maximum positive and negative changes in water storage shown in Figure 8 corresponds

DOI: 10.1002/hyp

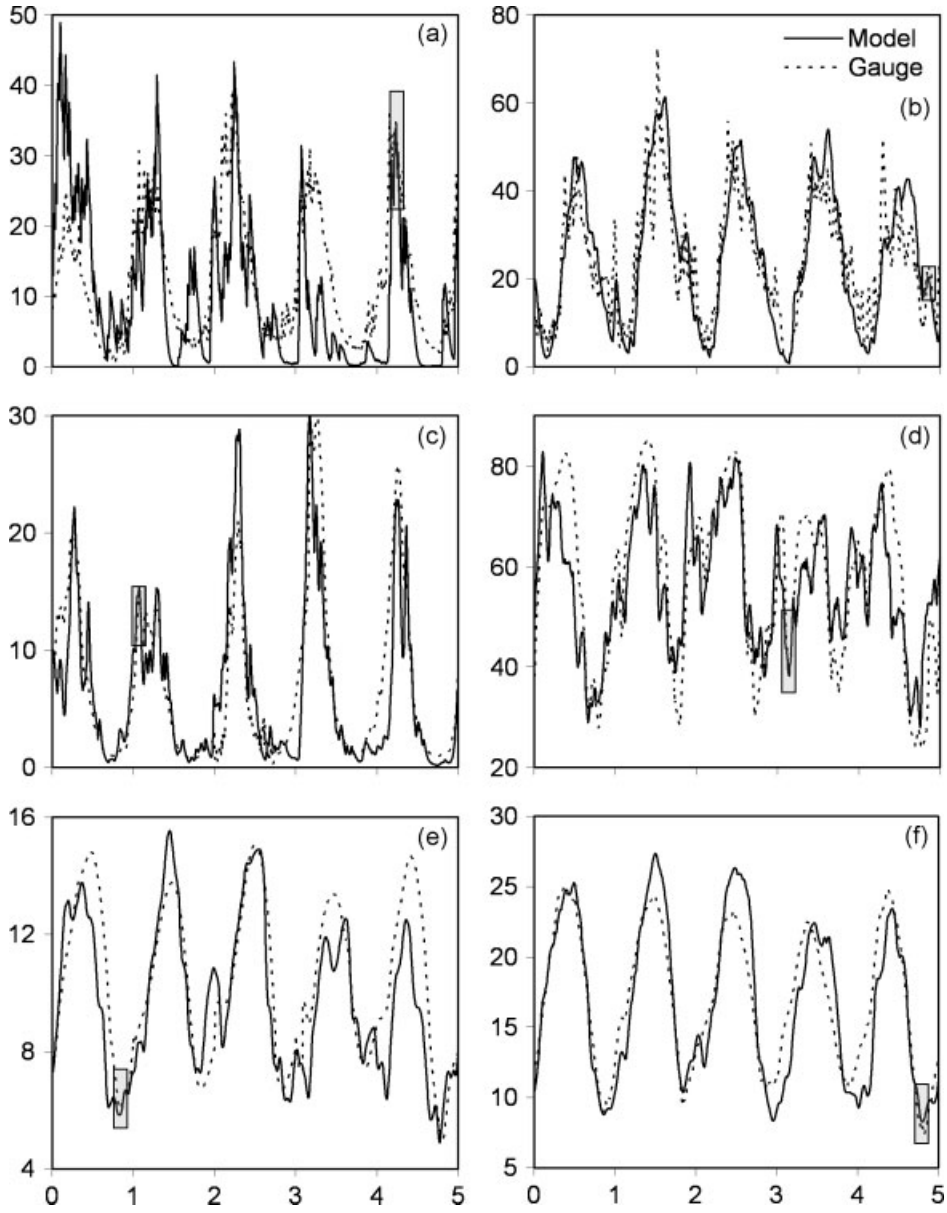

Figure 6. Comparison between daily simulated and gauged streamflow for the 5 year study period, x-axis: 1 Jan 2001–31 Dec 2005, at six gauge locations (gauge nos. listed in Table I): (a) 15575000 [0·005 million km^2, y-axis units 10s of m^3 s^{-1}]; (b) 14260000 [0·04 million km^2, 100s of m^3 s^{-1}]; (c) 18850000 [0·4 million km^2, 1000s of m^3 s^{-1}]; (d) 11500000 [1·1 million km^2, 1000s of m^3 s^{-1}]; (e) 14100000 [2·1 million km^2, 10 000s of m^3 s^{-1}]; and (f) 17050001 [4·7 million km^2, 10 000s of m^3 s^{-1}]

to the maximum positive and negative changes in channel/floodplain storage, which is also within a month of the maximum changes for the routable subsurface flows.

The fractional components of the basin-wide change in water storage are approximately 20% root-zone soil moisture, 40% subsurface water being routed laterally to channels, and 40% channel/floodplain discharge. Of particular interest is the simultaneity of the these three storages over time (Figure 9), which suggests that the north-south hemisphere climatic driver smears out any routing effects on storage when storage is totaled at the whole-basin scale. In other words, the Amazon's position on the equator, possibly coupled with its size keeps the total storage change within $+/-5$ cm month^{-1}, which is similar to the mean monthly variability in rainfall over the study period. The vertical error bars for the combined water storage changes suggests that the annual variability for a given monthly value is on the order of $+/-2{\cdot}5$ cm, where the maximum variability is shown for February ranging from $-3{\cdot}5$ to $+4{\cdot}5$ cm. This variability is mostly due to the timing of precipitation, where timing changes in the arrival of rainfall by $+/-$ a few weeks can increase or decrease the monthly basin-wide water storage changes by $+/-2{\cdot}5$ cm. For example, Figure 10 shows the mean cumulative rainfall starting in January for the five study years, and the monthly ranges in cumulative rainfall. The greatest monthly variability is in January–March and August–November, where the variation in cumulative monthly precipitation is approximately 8 to 11 cm. Assuming 50–60% is lost to *ET* within a month, that variability in basin water storage

DOI: 10.1002/hyp

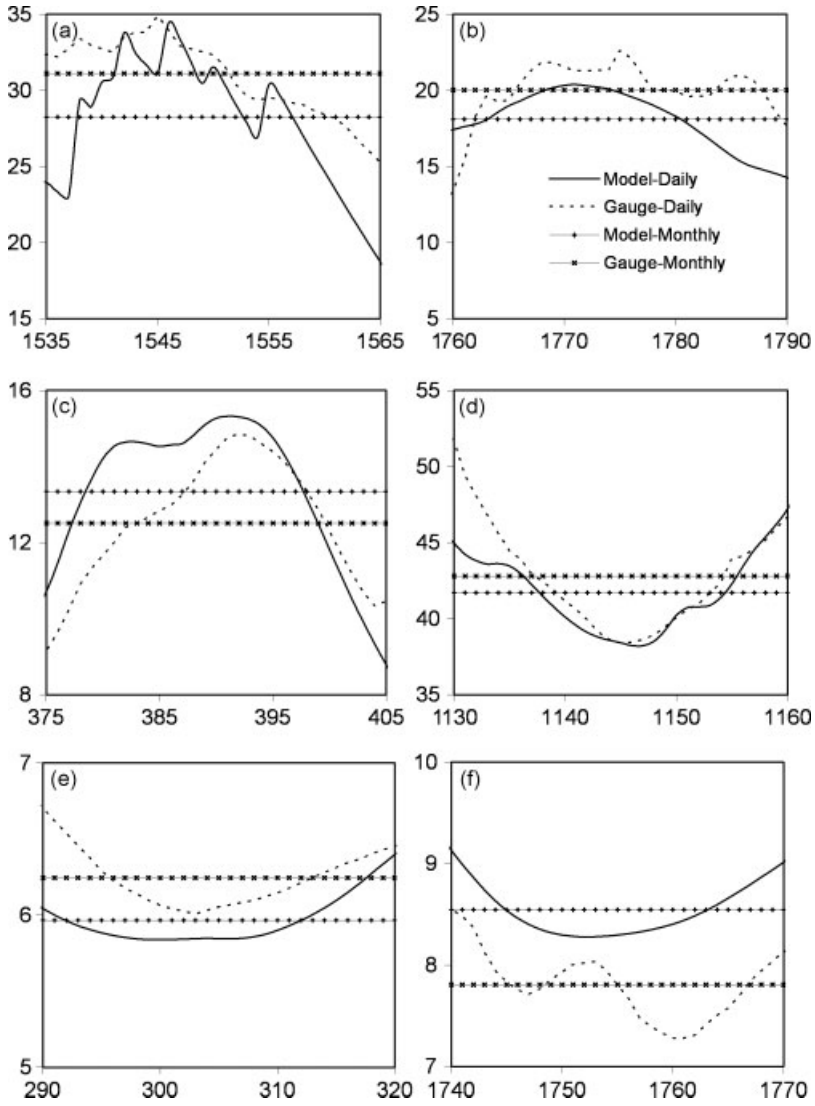

Figure 7. Comparison between daily and monthly simulated and gauged streamflow for select periods shown in highlighted boxes in Figure 6; x-axis in days from 1 Jan 2001, at six gauge locations (gauge nos. listed in Table I):): (a) 15575000 [0·005 million km^2, y-axis units 10s of m^3 s^{-1}]; (b) 14260000 [0·04 million km^2, 100s of m^3 s^{-1}]; (c) 18850000 [0·4 million km^2, 1000s of m^3 s^{-1}]; (d) 11500000 [1·1 million km^2, 1000s of m^3 s^{-1}]; (e) 14100000 [2·1 million km^2, 10 000s of m^3 s^{-1}]; and (f) 17050001 [4·7 million km^2, 10 000s of m^3 s^{-1}]

change is about +/−3 to 5 cm, which is similar to the range shown in Figure 9.

CONCLUSIONS

This paper presents a modelling framework based on a flexible representation of land surface topography and a fluvial transport system, that is capable of providing realistic channel and floodplain hydraulic characteristics on a daily time scale. The combined model can be used for systematically incorporating improvements in data availability, understanding of processes and for conducting computational experiments to understand the roles of large-scale drivers such as precipitation variations, geographic scale, and land surface condition on water availability in various parts of the hydrologic systems of large river basins. The framework integrates two models: (1) WBM for the vertical fluxes and stores of water in and through the canopy and soil layers, based on the conservation of mass and energy; and (2) a model for the horizontal routing of surface and subsurface runoff and channel and floodplain waters based on kinematic and diffusion wave methods. The models are driven by satellite-derived precipitation (TRMM_3B42) and air temperature (MOD08_M3). The model's use of an irregular computational grid, which limits the transfer of water between model elements to only nodes along the drainage network, is intended to facilitate parallel processing for applications to larger spatial and temporal domains.

Results for the Amazon Basin for the study period January 2001 to Decembetr 2005 are presented. The model is shown to capture annual runoff, annual peaks, seasonal patterns and daily fluctuations over a range of spatial scales (>1000 to <4·7 million km^2). By tracking all components of the water balance, root-zone storage, surface and subsurface runoff, and channel/floodplain discharges, the model can be used investigate the controls of basin-wide water storage changes, which can be

DOI: 10.1002/hyp

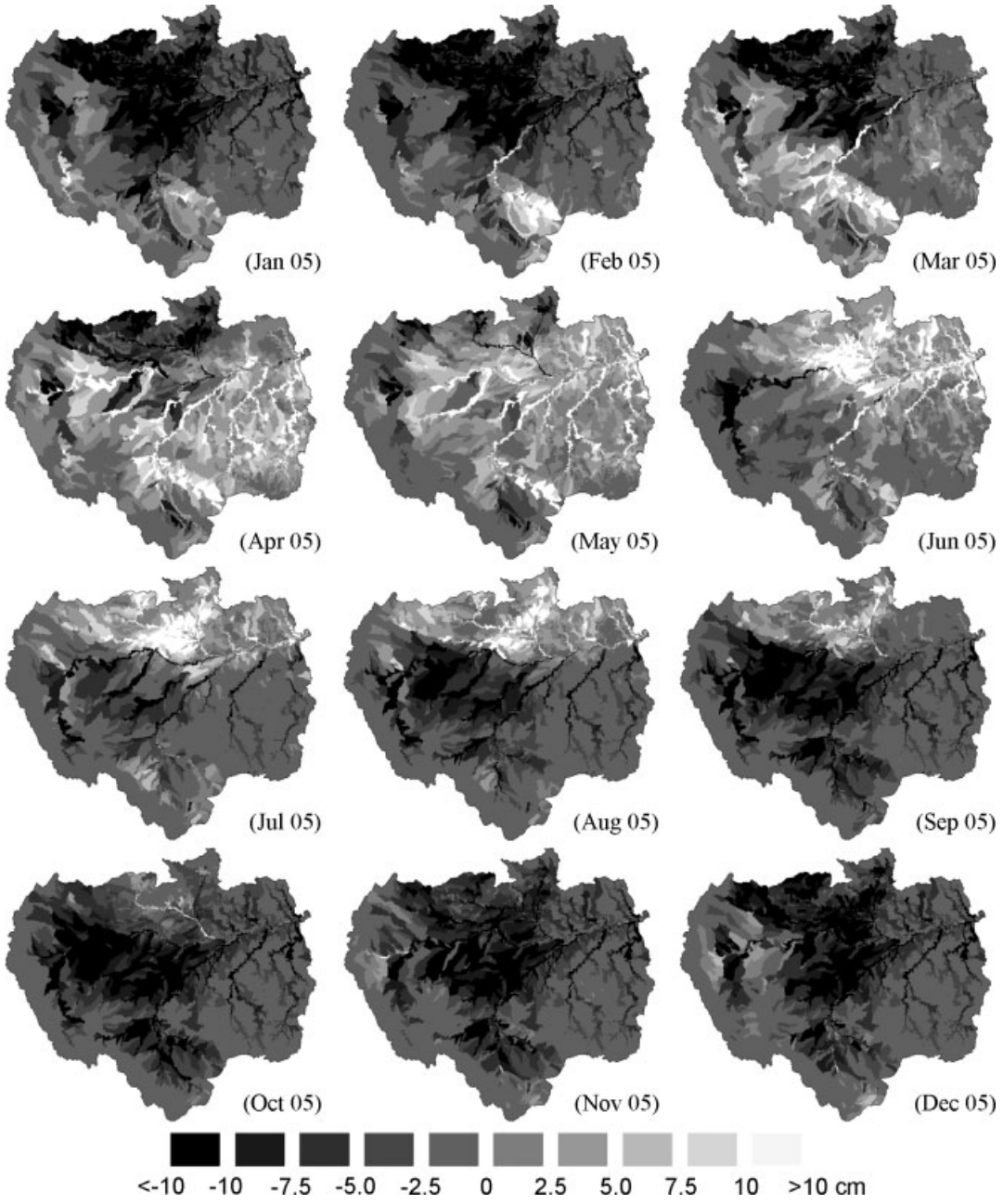

Figure 8. Change in total monthly water storage (cm) over the Amazon Basin for Jan 05—Dec 05 relative to the mean storage for the reference period Apr 02—Dec 03, where total water storage includes root zone soil moisture, surface and subsurface runoff, and channel and floodplain flow

detected by the GRACE satellite. For the period of study, results suggest water storage in the Amazon Basin varies by approximately +/−5 to 10 cm. The fractional components accounting for these changes are: root zone soil moisture (20%), subsurface water being routed laterally to channels (40%) and channel/floodplain discharge (40%). Annual variability in monthly water storage changes by +/−2·5 cm is likely due to 0·5 to 1 month viability in the arrival of significant rainfall periods throughout the basin.

ACKNOWLEDGEMENTS

In part, this work was carried out under the auspices of the NASA New Investigator Program, Contract No. NNX06AF13G; NASA Earth Observing System project NAG5-6120; NASA LBA project SH-02: NASA/NAG5-8396; US Geological Survey Contract No. 05CRAG0029; and the National Nuclear Security Administration of the US Dept. of Energy at Los Alamos National Laboratory under Contract No. DE-AC52-06NA25396; Los Alamos National Laboratory Directed Research and Development project, 'High-Resolution Physically-Based Model of Semi-Arid River Basin Hydrology', and US Dept. of Energy's Climate Change Prediction Program in the Office of Science. The authors thank Dr Rosangela Sviercoski for her analysis and extension of the discharge data at select stations in the Amazon basin. These data products were used in the basin model calibration.

DOI: 10.1002/hyp

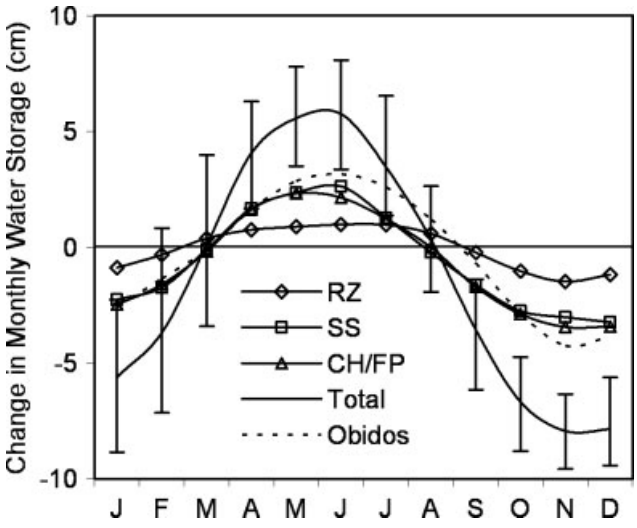

Figure 9. Mean monthly changes in total water storage over the 5 year study period, with vertical error bars showing the monthly range, and the three primary components: root-zone soil moisture (RZ), subsurface water being routed laterally (SS), and combined channel and floodplain flow (CH/FP); mean monthly discharge at Obidos in basin-wide units of depth shown as a dashed line

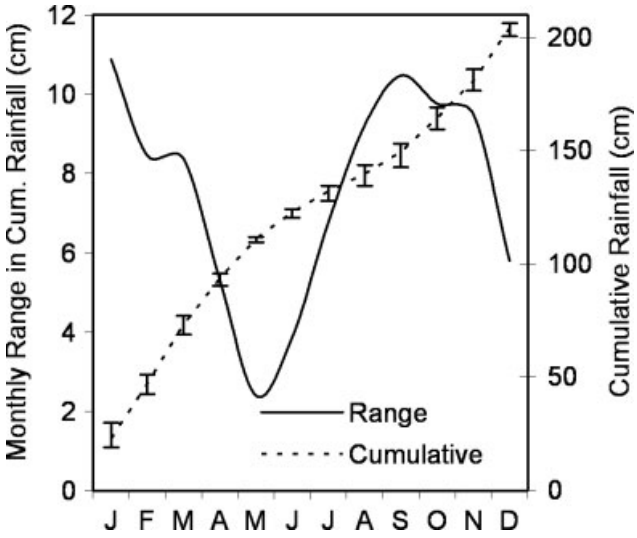

Figure 10. Mean monthly cumulative rainfall (TRMM_3B42) averaged over the Amazon Basin and range in monthly values over the 5 year study period

APPENDIX A: WATER BALANCE MODEL

Figure 4 shows the conceptual framework for the WBM. For each model unit, the WBM solves:

$$\Delta S_c + \Delta S_u = P - E_s - E_c - E_T - T_s - D \qquad \text{(A-1)}$$

where each term has units of [mm/timestep] and ΔS_c is the change in canopy water storage; ΔS_u is the change in the rooting zone water storage; P is precipitation; E_s is soil evaporation; E_c is canopy evaporation; E_T is transpiration; T_s is water available for surface runoff; and D is water transferred to the lower soil layer and is available for horizontal subsurface routing. The WBM passes T_s and D to the routing model, which performs the water balance in the lower soil layer.

The maximum canopy storage is defined as $S_{c,max} = \text{LAI} \cdot C_{max}$, where LAI is leaf area index and $C_{max} = 0{\cdot}2$ mm (Dickinson *et al.*, 1986). The maximum storage capacity for the upper soil layer is $S_{u,max} = h_{root}\ (\theta_f - \theta_w)$, where θ_f is soil moisture content at field capacity, θ_w is soil moisture at the permanent wilting point, and h_{root} is the thickness of the root zone. In this application, $\theta_f - \theta_w$ was calibrated as 10% ($\sim 0{\cdot}35 - 0{\cdot}25$), which agrees with the median (0·11) of a sample of 109 small-scale field measurements from the upper metre of soil in the western, eastern, and central Amazon basin that was accumulated from published values. The lower soil-saprolite layer is simulated in the routing model and supports horizontal transport to the channel network.

The WBM simulates processes on a daily timestep (Δt). For each day with precipitation, a fixed percentage of precipitation is intercepted by the canopy (calibrated: $f_i = 0{\cdot}15$) and available for canopy evaporation. If the canopy is still wet at the end of the time step, it is assumed that the canopy store is limited to the maximum value and the remaining water is released to the soil surface. When available, canopy storage is evaporated using the Penman–Monteith potential evaporation rate, E_p, with the surface resistance factor set to zero (Shuttleworth, 1993):

$$E_p = \frac{1}{\lambda}\left[\frac{\Delta R_N + \rho_a c_p (e_s - e)/r_a}{\Delta + \gamma(1 + (r_s \div r_a))}\right] \qquad \text{(A-2)}$$

where λ is the latent heat of vaporization, Δ is the slope of the saturated vapour pressure-temperature curve, R_N is the net radiation, ρ_a is the density of air, c_p is the specific heat of air, e_s is the saturated vapour pressure, e is the vapour pressure, γ is the psychrometric constant, r_a is the aerodynamic resistance factor, and r_s is the surface resistance factor. In this application, minimum and maximum air temperature and the latitude of the model unit are used to determine the require model parameters following the procedures outlined by Allen *et al.* (1998).

The potential evaporation rate with $r_s = 0$, $E_p{}^*$, is determined using Equation (A-2). $E_p{}^*$ is then used to determine the length of time during a time step for which the canopy is dry, T_d:

$$T_d = \min\lfloor 0, \Delta t - (S_c + P f_i)/E_p^* \rfloor \qquad \text{(A-3)}$$

If $T_d > 0$, then $S_c(t) = 0$. If $T_d = 0$, the only ET term is $E_p{}^*$ and canopy storage is determined by:

$$S_c(t) = [S_c(t-1) + P f_i] - E_p^* \cdot \Delta t \qquad \text{(A-4)}$$

If $S_c(t) = S_{c,max}$, the excess intercepted precipitation ((Equation (A-4))—$S_{c,max}$), is transferred to the soil surface as additional throughfall.

Next, the fraction of saturated soil surface, f_s, and the actual ET is determined by:

$$f_s = \alpha_{\min} + (\alpha_{\max} - \alpha_{\min}) \cdot (S_u \div S_{u,\max}) \qquad \text{(A-5)}$$

$$E_c = E_p{}^*\ \Delta t \qquad \text{(A-6)}$$

DOI: 10.1002/hyp

$$E_s = E_p{}^* \; T_d \; f_s \tag{A-7}$$

$$E_T = E_p \; T_d(1 - f_s) \tag{A-8}$$

where $\alpha_{\min}$ and $\alpha_{\max}$ are fractional areas of the landscape that define the range of model area that becomes saturated over the course of the year (assumed as 1 and 5%); E_c is constrained such that $E_c \leq (S_c(t-1) + P f_i)$; and $E_T + E_s$ is constrained to be $\leq (S_u(t) + \text{infiltration})$; f_s is used to split available energy between saturated surface evaporation and transpiration; and T_d accounts for energy lost to canopy evaporation. The combined set of equations and constraints ensures that the energy available for *ET* is conserved.

For application to the Amazon Basin, the resistance terms in Equation (A-2) are based on values for forested watersheds: $r_a = 33/U_2$ and $r_s = 30 \cdot f(\theta)/\text{LAI}$, where U_2 is wind speed at 2 m above the surface (assumed to be 5 m s^{-1}) and $f(\theta)$ is a stress factor that varies with soil moisture (Shuttleworth *et al*., 1984; Dickinson *et al*., 1986; Shuttleworth, 1993; Liang *et al*., 1994):

$$f(\theta) = \left[\frac{(\theta - \theta_w)}{(\theta_f - \theta_w)} \right] \tag{A-9}$$

Next, water available for surface runoff, infiltration, F, and the upper soil layer storage are determined:

$$T_s = (1 - P \; f_i) \; f_s \tag{A-10}$$

$$F = (1 - P \; f_i) - T_s \tag{A-11}$$

$$S_u(t) = \min [0, \; S_u(t-1) + F - E_T - E_S] \tag{A-12}$$

If $S_u(t) = 0$, the *ET* terms are reduced to balance the upper soil layer storage. If $S_u(t) > S_{u,max}$, $S_u(t)$ is set to $S_{u,max}$, and the excess water is transferred to the lower soil layer:

$$D = S_u(t-1) - F - E_s - E_T - S_{u,\max} \tag{A-13}$$

Finally, T_s and D are passed to the routing model for horizontal transport.

REFERENCES

Allen RG, Pereira LS, Raes D, Smith M. 1998. *Crop Evapotranspiration—Guidelines for Computing Crop Water Requirements, Irrigation and Drainage Paper No. 56*. Food and Agriculture Organization of the United Nations: Rome.

Alsdorf DE, Lettenmaier DP. 2003. Tracking fresh water from space. *Science* **301**: 1485–1488.

Alsdorf DE, Melack JM, Dunne T, Mertes LAK, Hess LL, Smith LC. 2000. Interferometric radar measurements of water level changes on the Amazon flood plain. *Nature* **404**: 174–177.

Alsdorf DE, Rodríguez E, Lettenmaier DP. 2007. Measuring surface water from space. *Reviews of Geophysics* **45**: RG2002, DOI:10·1029/2006RG000197.

Arcement GJ, Schneider VR. 1989. Guide for selecting Manning's roughness coefficients for natural channels and flood plains. United States Geological Survey, Water-supply Paper 2339.

Bates PD, Horritt MS, Smith CN, Mason D. 1997. Integrating remote sensing observations of flood hydrology and hydraulic modeling. *Hydrological Processes* **11**: 1777–1795.

Beighley RE, Moglen GE. 2003. Adjusting measured peak discharges from an urbanizing watershed to reflect a stationary land use signal. *Water Resources Research* **39**(4): 4·1–4·11, DOI:10·1029/2002WR001846.

Beven K. 2001. How far can we go in distributed hydrological modelling? *Hydrology and Earth System Sciences* **5**(1): 1–12.

Blöschl G, Sivapalan M. 1995. Scale issues in hydrological modeling: A review. *Hydrological Processes* **9**: 251–290.

Chow VT. 1959. *Open Channel Hydraulics*. McGraw-Hill: New York.

Coe MT. 2000. Modeling terrestrial hydrological systems at the continental scale: testing the accuracy of an atmospheric GCM. *Journal of Climate* **13**: 686–704.

Coe MT, Costa MH, Howard EA. 2008. Simulating the surface waters of the Amazon River basin: impacts of new river geomorphic and flow parameterizations. *Hydrological Processes* **22**: 2542–2553.

Costa MH, Foley JA. 1997. Water balance of the Amazon Basin: Dependence on vegetation cover and canopy conductance. *Journal of Geophysical Research* **102**(D20): 23 973–23 989.

Costa MH, Foley JA. 1998. A comparison of precipitation datasets for the Amazon basin. *Geophysical Research Letters* **25**: 155–158.

de Goncalves LGG, Shuttleworth WJ, Nijssen B, Burke EJ, Marengo JA, Chou SC, Houser P, Toll DL. 2006. Evaluation of model-derived and remotely sensed precipitation products for continental South America. *Journal of Geophysical Research* **111**: D16113.1–D16113.13, DOI:10·1029/2005JD006276.

de Moraes JM, Schuler AE, Dunne T, Figueiredo RO, Victoria RL. 2006. Water storage and runoff processes in plinthic soils under forest and pasture in Eastern Amazonia. *Hydrological Processes* **20**(12): 2509–2526.

Dickinson RE, Henderson-Sellers A, Kennedy PJ, Wilson MF. 1986. *Biosphere-atmosphere transfer scheme (BATS) for the NCAR community model*. NCAR Technical Note NCAR/TN-275+STR. National Center for Atmospheric Research: Boulder, Colorado.

Dunne T. 1978. Field studies of hillslope flow processes. In *Hillslope Hydrology*, Kirkby MJ (ed). Wiley: Chichester; 227–293.

Dunne T, Black RD. 1970. Partial-area contributions to storm runoff in a small New England watershed. *Water Resources Research* **6**: 1297–1311.

Dunne T, Dietrich WE. 1980. Experimental study of Horton overland flow on tropical hillslopes. Part II: Sheetflow hydraulics and hillslope hydrographs. *Zeitschrift für Geomorphologie*, Supplement Band **33**: 60–80.

Eagleson PS. 1970. *Dynamic Hydrology*. McGraw-Hill: New York.

Eggert KG. 1980. *A hydrologic simulation for predicting nonpoint source pollution*. PhD dissertation, Civil Engineering, Colorado State University, Ft. Collins, CO.

Eggert KG. 1987. Upstream calculations of characteristics for kinematic wave routing. *Journal of Hydraulic Engineering* **113**(6): 743–752.

Farr TG, Rosen PA, Caro E, Crippen R, Duren R, Hensley S, Kobrick M, Paller M, Rodriguez E, Roth L, Seal D, Shaffer S, Shimada J, Umland J, Werner M, Oskin M, Burbank D, Alsdorf D. 2007. The Shuttle Radar Topography Mission. *Reviews of Geophysics* **45**: RG2004, DOI:10·1029/2005RG000183.

Garbrecht J, Brunner G. 1991. Hydrologic channel-flow routing for compound sections. *Journal of Hydraulic Engineering* **117**(5): 629–642.

Grayson RB, Blöschl G, Western AW, McMahon TA. 2002. Advances in the use of observed spatial patterns of catchment hydrological response. *Advances in Water Resources* **25**: 1313–1334.

Goulding M. 1981. *Man and Fisheries on an Amazon Frontier*. W Junk: The Hague, Netherlands.

Gummadi V. 2008. *Hydraulic geometry relations for the Amazon Basin*. MS thesis, Civil, Construction and Environmental Engineering. San Diego State University, San Diego, CA.

Harley BM, Perkins FE, Eagleson PS. 1970. *A Modular Distributed Model of Catchment Dynamics*. *Hydrodynamics Report* No. 133, Massachusetts Institute of Technology: Cambridge, MA.

Hess LL, Melack JM, Novo EMLM, Barbosa CCF, Gastil M. 2003. Dual-season mapping of wetland inundation and vegetation for the central Amazon basin. *Remote Sensing of Environment* **87**: 404–428.

Huffman GJ, Adler RF, Bolvin DT, Gu G, Nelkin EJ, Bowman KP, Hong Y, Stocker EF, Wolff DB. 2007. The TRMM multi-satellite precipitation analysis: quasi-global, multi-year, combined-sensor precipitation estimates at fine scale. *Journal Hydrometeorology* **8**(1): 38–55.

Koster RD, Suarez MJ, Ducharne A, Stieglitz M, Kumar P. 2000. A catchment-based approach to modeling land surface processes in a GCM, Part 1: Model structure. *Journal of Geophysical Research* **105**: 24 809–24 822.

Li RM, Simons DB, Stevens MA. 1975. A nonlinear kinematic wave approximation for water routing. *Water Resources Research* **11**(2): 245–252.

Liang X, Lettenmaier DP, Wood EF, Burges SJ. 1994. A simple hydrologically based model of land surface water and energy fluxes for GCMs. *Journal of Geophysical Research* **99**(D7): 14 415–14 428.

Mahmood K, Yevjevich V. 1975. *Unsteady Flow in Open Channels*. Water Resources Press: Ft. Collins, CO.

Maidment D. 1992. *Handbook of Hydrology*. McGraw-Hill: New York.

Melack JM, Forsberg B. 2001. Biogeochemistry of Amazon floodplain lakes and associated wetlands. In *The Biogeochemistry of the Amazon Basin and its Role in a Changing World*, McClain ME, Victoria RL, Richey JE (eds). Oxford University Press: New York; 235–276.

Melack JM, Hess LL, Gastil M, Forsberg BR, Hamilton SK, Lima IBT, Novo EMLM. 2004. Regionalization of methane emissions in the Amazon basin with microwave remote sensing. *Global Change Biology* **10**: 530–544.

Mertes LAK, Dunne T. 2008. The effects of tectonics, climatic history, and sea-level history on the form and behavior of the modern Amazon River. In *Large Rivers,* Gupta A (ed). John Wiley and Sons; 115–144.

Moglen GE, Beighley RE. 2000. Using GIS to determine the extent of gaged streams in a region. *Journal of Hydrologic Engineering* **5**(2): 190–196.

Oki T, Sud YC. 1998. Design of total runoff integrating pathways (TRIP)—a global river channel network. *Earth Interactions* **2**: 1–37.

Oleson KW, Dai Y, Bonan G, Bosilovich M, Dickinson R, Dirmeyer P, Hoffman F, Houser P, Levis S, Niu GY, Thornton P, Vertenstein M, Yang ZL, Zeng X. 2004. Technical Description of Community Land Model (CLM), NCAR Technical Note NCAR/TN-461+STR, National Center for Atmospheric Research, Boulder, CO.

Pfafstetter O. 1989. Classification of Hydrographic Basins; Coding Methodology, Departamento Nacional do Obras de Sanearnento, Rio de Janeiro, Brazil. [Translated by Verdin JP. U.S. Bureau of Reclamation: Denver, CO; 13].

Ponce VM, Yevjevich V. 1978. Muskingum-Cunge method with variable parameters. *Journal of the Hydraulics Division* **104**(12): 1663–1667.

Rawls WJ, Brakensiek DL, Miller N. 1983. Green–Ampt infiltration parameters from soils data. *Journal of Hydraulic Engineering* **109**(1): 62–70.

Richey J E, Mertes LAK, Dunne T, Victoria RL, Forsberg RB, Tancredi ACMS., Oliveira E. 1989. Sources and routing of the Amazon River flood wave. *Global Biogeochemical Cycles* **3**: 191–204.

Richey JE, Melack JM, Aufdenkampe AK, Ballester VM, Hess LL. 2002. Outgassing from Amazonian rivers and wetlands as a large tropical source of atmospheric CO2. *Nature* **416**: 617–620.

Rodell M, Famiglietti JS. 1999. Detectability of variations in continental water storage from satellite observations of the time-variable gravity field. *Water Resources Research* **35**(9): 2705–2723.

Seemann SW, Li J, Menzel WP, Gumley LE. 2003. Operational retrieval of atmospheric temperature, moisture, and ozone from MODIS infrared radiances. *Journal of Applied Meteorology* **42**: 1072–1091.

Shuttleworth WJ. 1993. Evaporation. In *Handbook of Hydrology*, Maidment DR (ed.). McGraw-Hill; 4·1–4·53.

Shuttleworth WJ, Gash JH, Lloyd CR, Moore CJ, Roberts J. 1984. Eddy correlation measurements of energy partition for Amazonian forest. *Quarterly Journal of the Royal Meteorological Society* **110**: 1143–1162.

Sippel SJ, Hamilton SK, Melack JM. 1991. Inundation area and morphometry of lakes on the Amazon River floodplain, Brazil. *Archives of Hydrobiology* **123**: 385–400.

Tapley BD, Bettadpur S, Ries JC, Thompson PF, Watkins MM. 2004. GRACE measurements of mass variability in the earth system. *Science* **305**(5683): 503–505.

Verdin KL, Verdin JP. 1999. A topological system for delineation and codification of the earth's river basins. *Journal of Hydrology* **218**: 1–12.

Vorosmarty CJ, Willmott CJ, Choudhury BJ, Schloss AL, Stearns TK, Robeson SM, Dorman TJ. 1996. Analyzing the discharge regime of a large tropical river through remote sensing, ground-based climate data and modeling. *Water Resources Research* **32**(1): 3137–3150.

Wooding RA. 1965. A hydraulic model for the catchment-stream problem: I. Kinematic wave theory. *Journal of Hydrology* **3**: 254–267.

Webb RW, Rosenzweig CE, Levine ER. 2000. Global Soil Texture and Derived Water-Holding Capacities. Oak Ridge National Laboratory Distributed Active Archive Center [http://www.daac.ornl.gov]: Oak Ridge, TN, DIO:10·3334/ORNLDAAC/548.

Yang W, Tan B, Huang D, Rautiainen M, Shabanov NV, Wang Y, Privette JL, Huemmrich KF, Fensholt R, Sandholt I, Weiss M, Ahl DE, Gower ST, Nemani RR, Knyazikhin Y, Myneni RB. 2006. MODIS leaf area index products: from validation to algorithm improvement. *IEEE Transactions on Geoscience and Remote Sensing* **44**(7): 1885–1898.